Effects of temperature, nitrogen, and light limitation on the optical properties of the marine diatom *Thalassiosira pseudonana*

Dariusz Stramski

Marine Physical Laboratory, Scripps Institution of Oceanography, University of California at San Diego, La Jolla, California 92093-0238

Antoine Sciandra and Hervé Claustre

Laboratoire d'Océanographie de Villefranche, CNRS/Université Pierre et Marie Curie, B.P. 28, 06238 Villefranche-sur-Mer, France

Abstract

A series of laboratory experiments were conducted to examine the optical properties of the marine diatom *Thalassiosira pseudonana* for a broad range of growth rates (μ from 0.22 to 2 d^{-1}) under temperature-, nitrogen-, and light-limited conditions. The effects of temperature and nitrogen limitation on spectral absorption cross-sections expressed on a per cell basis, $\sigma_a(\lambda)$, were similar. With the reduction in growth rate, σ_a at a light wavelength $\lambda = 674$ nm showed an equivalent decrease regardless of whether the cells were limited by temperature or nitrogen. The effect of growth irradiance was distinctively different, since σ_a increased with light limitation. The chlorophyll *a* (Chl *a*)–specific absorption coefficient showed the opposite trends than those of σ_a. These patterns resulted primarily from the acclimative strategies of *T. pseudonana* involving an increase in Chl *a* content in response to light limitation and a decrease in Chl *a* under temperature and nitrogen limitation. The scattering cross-sections, $\sigma_b(\lambda)$, and carbon-specific scattering coefficients, $b_C^*(\lambda)$, were generally not a strong function of growth rate with the exception of lower values of b_C^* for light-limited cells. While *T. pseudonana* exhibited some changes in cell size, variations in the refractive index had the major influence on cell optical properties. The imaginary part of the refractive index (at $\lambda = 674$ nm) showed a strong correlation with intracellular Chl *a* concentration, and the real part of the refractive index (at $\lambda = 660$ nm) was correlated with the intracellular carbon concentration. Our results indicate that integrated studies of the effects of various environmental factors such as light, nutrients, and temperature are needed to adequately describe optical variability in phytoplankton.

It is widely recognized that phytoplankton exert a strong influence on light absorption and scattering in the upper ocean. Variability in the optical properties of the phytoplankton may result from changes in the composition of the community and also from changes in the optical properties of individual cells comprising the population of any species. The latter reflects the fact that phytoplankton cell size, shape, chemical composition, and hence refractive index, can change in response to the ambient growth conditions. Much of the previous research on the influence of light, nutrients, and temperature on phytoplankton optical properties was focused on absorption, fluorescence, or both (e.g., Kiefer 1973; Sosik and Mitchell 1994; Moore et al. 1995). Studies of light scattering by phytoplankton have typically been undertaken with no simultaneous measurements of absorption (e.g., Volten et al. 1998; Balch et al. 1999) or with little regard for the effects of growth conditions (e.g., Bricaud et al. 1988; Ahn et al. 1992). Few studies that included concurrent determinations of absorption and scattering by phytoplankton under varying growth conditions showed significant varia-

tions in both the absorption and scattering properties of phytoplankton cells (Stramski and Morel 1990; Stramski and Reynolds 1993; Reynolds et al. 1997). A lack of comprehensive optical studies for a wide range of species and growth conditions remains, however, a major obstacle to a better understanding of the roles played by phytoplankton in optical variability in the ocean. In this work we examine how limitation of growth by temperature, nitrogen, and light influences the absorption and scattering properties of *Thalassiosira pseudonana.*

Materials and methods

Experimental design—Laboratory experiments were conducted with the centric diatom *Thalassiosira pseudonana* (clone 3H) obtained from Provasoli-Guillard National Center for Culture of Marine Phytoplankton. The effect of temperature T ranging from 7 to 25°C was studied in batch cultures under light-saturating and nitrogen-replete conditions (Table 1). The effect of light was studied in nitrogen-replete batch cultures at a temperature of 25°C (Table 1). To examine the effect of nitrate limitation, two experiments were carried out at 20°C and saturating irradiance in continuous (chemostat) cultures (Table 1). Finally, a few additional experiments were made in N-replete medium at PAR = 40–60 μmol quanta m^{-2} s^{-1} and $T = 20$ and 25°C (not shown in Table 1). Data from these additional experiments are excluded from our discussion unless specifically indicated.

Table 1. Summary of growth conditions used in our experiments. The number of replicate experiments made at various temperatures T at low and high light levels are given. Nitrate conditions are indicated in parentheses. The average PAR values for low light and high light conditions are also given. The range of PAR for high light conditions corresponds to saturating irradiances (see *Fig. 8* for variations in PAR among replicate experiments at various temperatures).

T (°C)	Low light PAR ~24 (μmol quanta m^{-2} s^{-1})	High light PAR ~330–410 (μmol quanta m^{-2} s^{-1})
7		2 (N replete)
10		3 (N replete)
15		3 (N replete)
20		5 (N replete)
20		2 (N limited)
25	3 (N replete)	3 (N replete)

The culture vessels consisted of water jacketed 2-liter cylinders connected to a circulating water bath that maintained constant temperature (± 0.05°C about the desired value). The growth medium was prepared using 0.22-μm Millipore filtered and autoclaved (105°C for half an hour) seawater and nutrient enrichments according to f/2 formulation (Guillard and Ryther 1962). After cooling and sterile addition of nutrients, the medium was transferred to the culture vessels through a 0.22-μm sterile filter (MediaKap-5, Microgon). The concentration of NO$_3$ in fresh media prepared for the batch experiments was 130 μM. For the chemostat experiments this concentration was 60 μM. The chemostat cultures were operated at a dilution rate corresponding to the growth rate of 0.5 d^{-1}. Both the batch and chemostat cultures were subject to continuous gentle stirring and bubbling with sterile-filtered air, which passed through a 0.1-μm Whatman filter and activated charcoal at a rate of 0.15 liter per minute.

The cultures were grown under continuous illumination from 150W metal halide lamps (HQI, Osram), which provide a high output with a relatively flat spectral distribution of light (Bernard et al. 1996). The lamp assembly was located above the culture vessels and was equipped with the UV-protecting glass screen. A 1-cm thick Plexiglas was placed between the lamps and the cultures to cut off the residual UV energy. The desired irradiances were obtained by adjusting the position of the lamps and by placing neutral density screens between the lamps and culture vessels. Photosynthetically available radiation (PAR) was measured with a quantum scalar irradiance meter (QSL-100, Biospherical Instruments) by immersing the spherical collector in the culture.

We monitored detailed evolution of the cultures between the inoculation of the medium until the time of optical measurements, and then for one more day or so after these measurements (Fig. 1). Specifically, the NO$_3$ concentration within the medium was measured twice a day in batch cultures and more frequently in continuous cultures. The cell concentration and cell size distribution were measured at least 6 times a day and as frequently as 12 times a day throughout the experiments. This information was essential for determining the optimum time for optical measurements, which
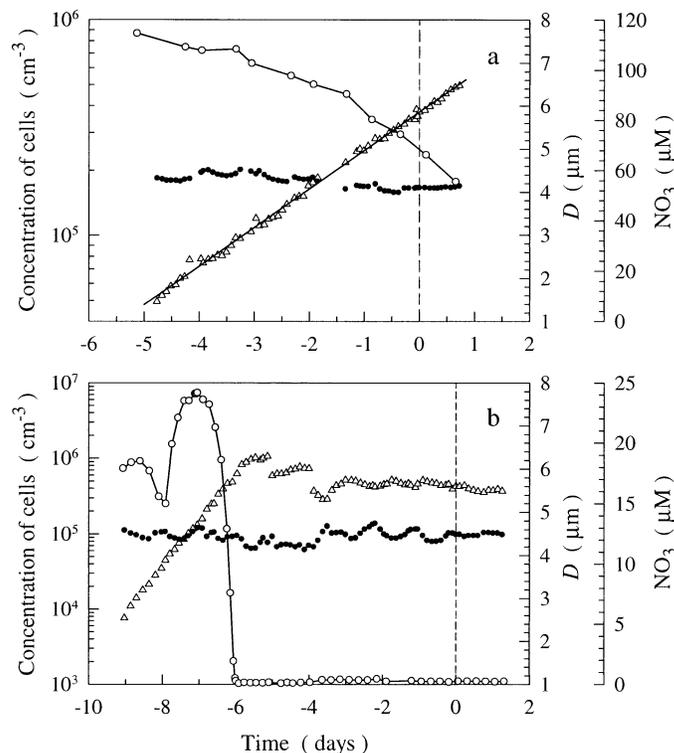

Fig. 1. Time series of cell concentration (triangles), nitrate concentration NO$_3$ (open circles), and mean cell diameter D (solid circles) for (a) the batch culture of *T. pseudonana* grown at 10°C under saturating irradiance in a nutrient-replete medium and (b) the chemostat culture grown at 20°C under saturating irradiance. The vertical dashed lines at time 0 indicate the sampling time for optical measurements and other analyses.

require a cell concentration that is high enough to ensure a sufficiently large signal-to-noise ratio in optical measurements over a 1-cm pathlength, but low enough to avoid multiple photon-particle interactions over that pathlength. The beam attenuation coefficient of the cultures at the time of analysis was less than 30 m^{-1} (usually $<$20 m^{-1}), which corresponds to the photon mean free path greater than 3.3 cm (usually $>$5 cm).

Nutrient measurements—Nitrite NO$_2$ and nitrate NO$_3$ concentrations were measured with a Technicon Auto-analyzer and an automated data acquisition system (Malara and Sciandra 1991). These measurements allowed us to verify that the batch cultures were N-replete and the continuous cultures were N limited.

Particle counting and sizing—The concentration and size distribution of cells were measured with an optical particle counter using the principle of light blockage (Hiac/Royco, Pacific Scientific Instruments). The system consists of three basic components: an automated liquid syringe particle sampler (Model 3000), a laser diode sensor (HRLD-400HC), and a high-speed digital counter (Model 9064). The measurements were analyzed with the Hiac particle distribution analysis software (PDAS). The instrument was calibrated with latex microspheres of 12 different sizes ranging from 1.5 to

250 μm. This calibration could potentially lead to some bias in our application because the latex particles have higher refractive index than phytoplankton cells. Nevertheless, tests with various phytoplankton species showed that the size distributions from the Hiac system are similar to those obtained with the Coulter particle analyzer.

Before counting and sizing of *T. pseudonana,* the cultures were diluted with an automated, computer-controlled system consisting of peristaltic pumps, solenoid valves, and a syringe (Bernard et al. 1996). We worked with as many as six cultures at a time. These cultures were analyzed with the Hiac system 6 to 12 times a day, and each analysis consisted of triplicate measurements taken in rapid succession. The coefficient of variation for these replicates was less than 3%, and these data were subsequently averaged. The mean cell diameter, *D,* geometrical cross-section, *G,* and volume, *V,* were calculated from the size distribution (e.g., Stramski and Reynolds 1993). The total biovolume was calculated from the product of *V* and the cell concentration.

Determinations of carbon, nitrogen, and chlorophyll a— To determine the concentration of particulate organic carbon (POC) and particulate organic nitrogen (PON) of the cultures, triplicate samples of 40 ml were filtered onto precombusted glass fiber filters (Whatman GF/F), dried at 60°C, and analyzed with a LECO 900 CHN analyzer. The replicates agreed typically to within 5%. For chlorophyll *a* (Chl *a*) determinations, 20-ml samples were filtered onto GF/F filters, which were subsequently stored in liquid nitrogen until high-performance liquid chromatography (HPLC) analysis as described in Vidussi et al. (1996). Extraction was performed in 3 ml of cold methanol containing a known amount of Zn(II) pyropheophorbide octadecyl ester as internal standard (Mantoura and Repeta 1997). The extraction efficiency was improved by sonication for 30 s, and the extract was then clarified by filtration through Whatman GF/C filters. The coefficient of variation for Chl *a* concentration between replicate samples was, on average, 6%.

Because of a failure in the ultra-low temperature system for sample storage, the number of samples available for the HPLC analysis was limited to 12. These samples covered the whole range of the examined growth conditions and included replicate samples of temperature-limited cells grown at the lowest temperature of 7°C, light-limited cells grown at 20 and 25°C in N-replete medium, N-limited cells from the chemostat experiment, and, finally, cells grown under optimal conditions of temperature, saturating light, and N-replete medium. These measurements were used to establish a relationship between the intracellular Chl *a* concentration and the imaginary part of the refractive index of cells. As described below, this relationship is excellent over the entire range of growth conditions and, therefore, was used to estimate Chl *a* for the experiments at intermediate temperatures lacking direct HPLC measurements.

The intracellular concentrations of Chl *a* (*Chl a_i*), carbon (*C_i*), and nitrogen (*N_i*) were calculated as a ratio of the respective concentrations of Chl *a,* POC, and PON in cell suspension to the total biovolume. The Chl *a,* carbon, and nitrogen contents per cell, denoted as *Chl a_c, C_c,* and *N_c,* respectively, were obtained by normalizing the Chl *a,* POC, and PON concentrations in cell suspension to the cell concentration.

Growth rate determinations—In the batch cultures, the growth rate μ was calculated from variations in the total biovolume during the exponential phase of growth over a time period of 2 to 7 d (depending on the experiment), including the time of sampling for optical and cell quota measurements. In the continuous cultures, sampling for optical and cell quota measurements was performed 5 to 6 d after the depletion of nitrate in the medium, and about 3 d after the establishment of a steady-state cell population. At this time, the growth rate was considered equal to the dilution rate of the cultures.

Determinations of optical properties—The spectral absorption coefficient, $a(\lambda)$, and the beam attenuation coefficient, $c(\lambda)$, were measured on cell suspensions in 1-cm quartz cuvettes with a dual beam spectrophotometer equipped with an integrating sphere (Perkin-Elmer Lambda 19). Measurements were made in the spectral region between $\lambda = 350$ nm and $\lambda = 750$ nm at 1-nm intervals. Filtered media from the cultures (0.2-μm syringe filter, Nalgene) were used as the reference. The concentration of cells in these measurements ranged from 3.6×10^5 to 5.3×10^5 cm^{-3}. Triplicate absorption and beam attenuation scans for each sample showed a very good reproducibility and were averaged to produce the final spectra. A 5-nm moving average was used to smooth the individual scans.

Special geometric configurations of the instrument were used to measure the absorption, $a(\lambda)$, and beam attenuation, $c(\lambda)$, coefficients as detailed elsewhere (e.g., Bricaud et al. 1983; Stramski and Reynolds 1993). Briefly, $a(\lambda)$ was measured by placing the cuvettes at the entrance to an integrating sphere that minimized losses due to light scattering. The value measured at 750 nm was subtracted from measurements at all wavelengths, which is a reasonable correction for the scattering error in such determinations of absorption by *T. pseudonana* (Reynolds et al. 1997). To measure $c(\lambda)$, the cuvettes were placed at some distance from the detector, and field stops were aligned within the lightpath to reduce the acceptance angle of the receiving aperture to less than 1°. The scattering coefficient, $b(\lambda)$, was calculated as the difference between $c(\lambda)$ and $a(\lambda)$.

The optical coefficients of cell suspensions were used in conjunction with the data for cell concentration and size distribution to calculate the optical properties at the level of a single cell. Optical cross-sections for absorption, $\sigma_a(\lambda)$, scattering, $\sigma_b(\lambda)$, and attenuation, $\sigma_c(\lambda)$, were obtained by normalizing the bulk coefficients, $a(\lambda)$, $b(\lambda)$, and $c(\lambda)$, respectively, to the cell concentration. The efficiency factors for absorption, $Q_a(\lambda)$, scattering, $Q_b(\lambda)$, and attenuation, $Q_c(\lambda)$, were calculated as a ratio of the respective optical cross-section to the mean geometrical cross-section of the cell, G. These single-particle optical properties represent a hypothetical mean cell derived from the actual population. The refractive index of the cells relative to water, including the real part of the index $n(\lambda)$ and the imaginary part $n'(\lambda)$, was estimated from an inverse method that uses the experimental data of the optical efficiency factors and cell size distribution
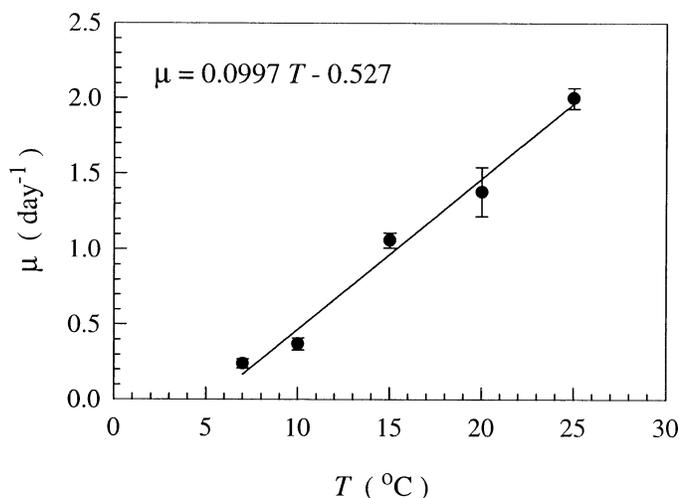
Fig. 2. Specific growth rate, μ, as a function of temperature, T, for *T. pseudonana* grown under saturating light and nutrient-replete conditions. The average value and standard deviation of μ at each temperature, the regression line, and the regression equation are shown. The squared correlation coefficient r^2 is 0.95 (the total number of observations is 16).
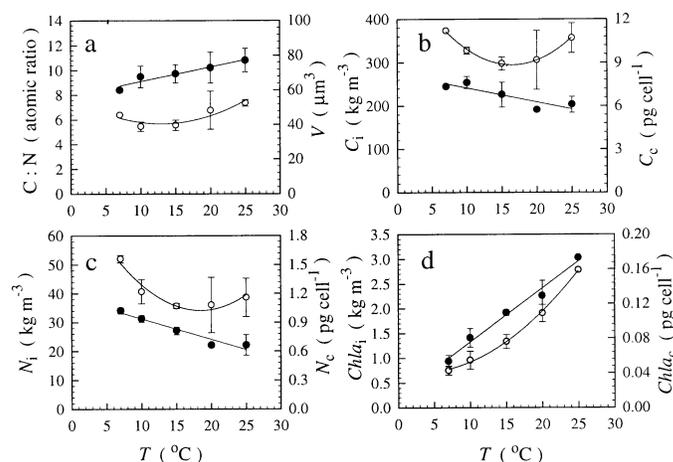
$$\mu = 0.0997\,T - 0.527$$

Fig. 3. The responses of cellular properties to variations in temperature for *T. pseudonana* grown under saturating light and nutrient-replete conditions. (a) Carbon-to-nitrogen ratio, C:N (solid circles), and mean cell volume, V (open circles). (b) Carbon content per cell, C_c (open circles), and intracellular concentration of carbon, C_i (solid circles). (c) Nitrogen content per cell, N_c (open circles), and intracellular concentration of nitrogen, N_i (solid circles). (d) Chl a content per cell, $Chl\,a_c$ (open circles), and intracellular concentration of Chl a, $Chl\,a_i$ (solid circles). The Chl a values for intermediate temperatures were derived from the imaginary part of the refractive index (*see* text and Fig. 10 for details). The average value and standard deviation is shown for each variable at each temperature. The data points are accompanied by trend lines.

as inputs to the theoretical formula for $Q_a(\lambda)$ of van de Hulst (1957) and Mie scattering calculations for homogeneous spheres (Bohren and Huffman 1983). The estimation of $n'(\lambda)$ is detailed in Bricaud and Morel (1986). The method for estimating $n(\lambda)$ is similar to that described in Stramski et al. (1988), with the exception that Mie scattering calculations, instead of the van de Hulst approximation, were used in the iterative process.

By normalizing the final spectra of optical cross-sections, $\sigma_a(\lambda)$, $\sigma_b(\lambda)$, and $\sigma_c(\lambda)$, to the cellular *Chl* a_c, C_c, and N_c representing each experiment, we also calculated the Chl a-, carbon-, and nitrogen-specific optical coefficients. In this paper, we will discuss variations in the Chl a–specific absorption, $a^*_{\mathrm{Chl}}(\lambda)$, and C-specific scattering, $b^*_{\mathrm{C}}(\lambda)$, coefficients.

Results

Effects of temperature—We found a linear dependence of growth rate, μ, on temperature, T (Fig. 2), consistent with results of Brand et al. (1981), who studied 14 clones of *T. pseudonana* at temperatures between 12 and 24°C. The values of μ in our experiments are similar to those reported by Thompson et al. (1992) for the same species.

Cell volume was smallest at $T = 10$°C and largest at 25°C (Fig. 3a). The size distribution at 25°C is clearly shifted toward larger equivalent cell diameters compared to the distribution obtained at 7°C (Fig. 4). The modal diameter of these distributions is 4.12 and 4.46 μm at 7 and 25°C, respectively. The distributions are similar to those measured previously on the same species with a Coulter counter (Reynolds et al. 1997).

While the intracellular concentration of organic carbon, C_i, and nitrogen, N_i, showed quite steady declines with temperature, the cellular content of these elements, C_c and N_c, exhibited broad U-shaped patterns with a minimum at inter-

mediate temperatures (Fig. 3b,c). Temperature had a greater effect on N_i than C_i. As a result, the C:N ratio increased with temperature (Fig. 3a). Chl a quotas increased more than threefold (Fig. 3d), and the carbon-to-Chl a ratio decreased from about 262 to 67 (by weight) over the temperature range of 7 to 25°C.

Variation in the imaginary part of the refractive index, n',
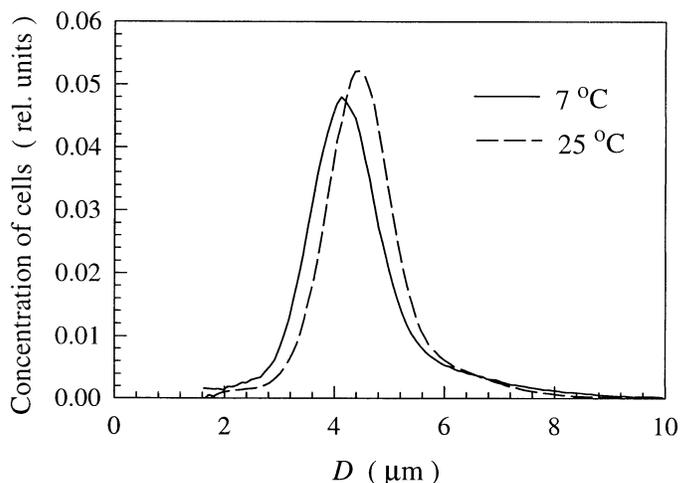

Fig. 4. Density functions of size distribution of *T. pseudonana* cells grown at 7 and 25°C under saturating irradiance and nutrient-replete conditions. For comparison, the distributions have been normalized to the total concentration of cells so that the integral of the presented functions over the entire size range is the same.
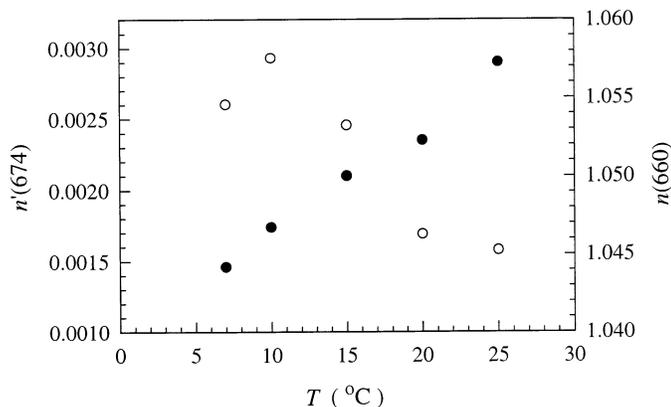
Fig. 5. The imaginary part of the refractive index (n') at 674 nm (solid circles) and the real part of the refractive index (n) at 660 nm (open circles), as a function of temperature for *T. pseudonana* cells grown under saturating irradiances and nutrient-replete conditions. The values of $n'(674)$ and $n(660)$ were derived from the average size distribution and average optical efficiency factors at each temperature (*see* text for details).

within the absorption peak of Chl *a* in the red (at $\lambda = 674$ nm) as a function of temperature (Fig. 5) was similar to that of the intracellular Chl *a* concentration. Because of the relationship between μ and T shown in Fig. 2, $n'(674)$ also increases linearly with temperature-dependent growth rate (not shown here). The real part of the refractive index, n, showed a significant decline with increasing temperature (Fig. 5). This pattern resembles variation in the intracellular carbon concentration C_i (*see* Fig. 3b).

Both the magnitude and spectral shape of the absorption cross-section changed in response to variations in cellular pigment content and cell size as a function temperature (Fig. 6). Slowly growing cells at low temperatures showed significantly smaller values for the absorption cross-sections $\sigma_a(\lambda)$ than cells growing rapidly at higher temperatures. This results primarily from a trend for intracellular pigment concentration, and hence n', to increase with increasing temperature (*see* Figs. 3 and 5). In the red absorption band of Chl *a*, $\sigma_a(674)$ increased more than twofold between 7 and 25°C (Fig. 6b). In the blue band at 438 nm, the corresponding increase was only 31%, but this increase may not be significant given that the standard deviation at higher temperatures is quite large. In any event, the blue-to-red absorption ratio decreased with the increase in temperature. This flattening of the spectrum can be partly attributed to the package effect, which is expected to be stronger in the blue than in the red (Morel and Bricaud 1981) and also to changes in the amounts of accessory pigments, especially carotenoids, relative to Chl *a*. In contrast to $\sigma_a(\lambda)$, Chl *a*–specific absorption coefficients, $a_{Chl}^*(\lambda)$, at 25°C were reduced compared to those at 7°C (not shown here) because the cellular Chl *a* increased to greater extent between 7 and 25°C than the absorption cross-sections.

The shape of spectral scattering cross-sections, $\sigma_b(\lambda)$, showed a general trend of scattering to increase with increasing wavelength (Fig. 7a). Superposed on this general pattern are spectral features associated with the major absorption bands in the blue and red spectral regions. These features
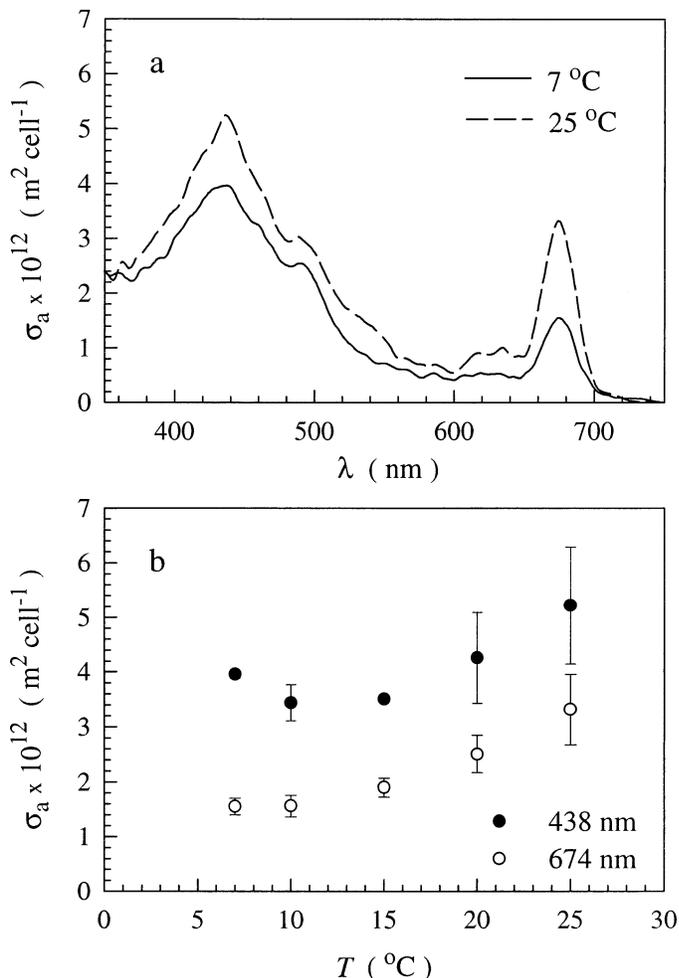

Fig. 6. Absorption cross-section of *T. pseudonana* grown under saturating irradiances and nutrient-replete conditions as a function of temperature. (a) Comparison of the average absorption cross-section spectra, $\sigma_a(\lambda)$, at temperatures of 7 and 25°C. (b) Absorption cross-section, at two wavelengths 438 nm and 674 nm, as a function of temperature. The average value and standard deviation is shown at each temperature.

are more pronounced for cells grown at high temperature because these cells have higher cellular pigment content and higher absorption than cells growing slowly at low temperature. As shown in Fig. 7a, the magnitude of variation of scattering with wavelength can differ noticeably depending on temperature, but no consistent pattern was found over the entire range of temperatures examined in this study. Nevertheless, $\sigma_b(\lambda)$ varied within a relatively narrow range of values in response to varying temperature, which results from the combined effect of cell size and refractive index (*see* opposite patterns in V and n in Figs. 3a and 5, respectively). For example, $\sigma_b(660)$ at various temperatures varied by <10% from the overall average value of $\sigma_b(660)$ (Fig. 7b). Similarly, the carbon-specific scattering coefficients, $b_C^*(\lambda)$, are not a strong function of temperature (not shown here). This is because the temperature-dependent patterns of C_c and σ_b are similar (*see* Figs. 3b and 7b, respectively). The
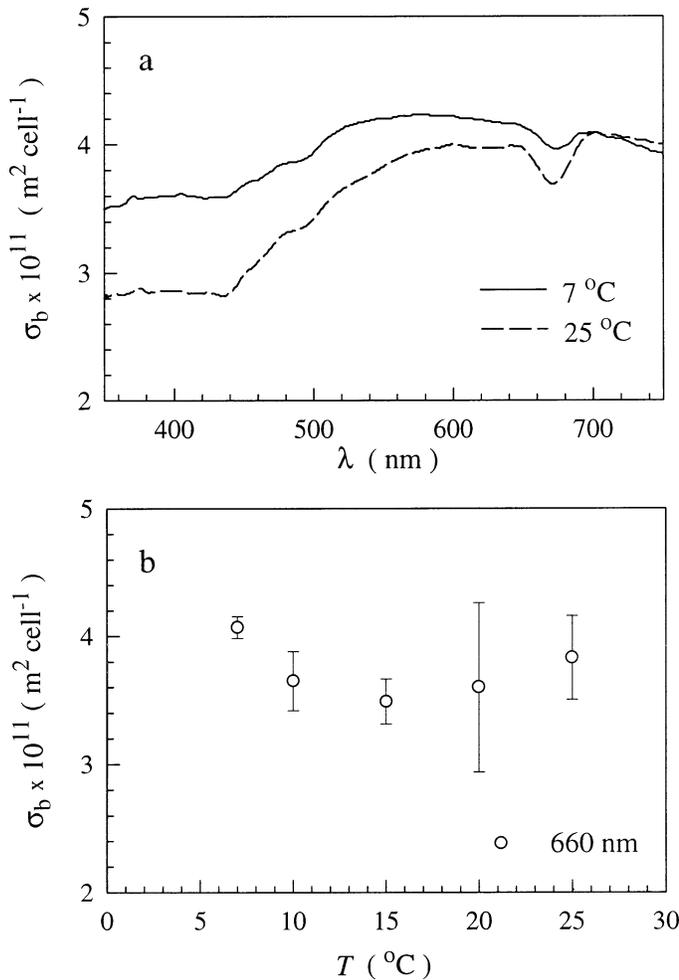
Fig. 7. Scattering cross-section of *T. pseudonana* grown under saturating irradiances and nutrient-replete conditions as a function of temperature. (a) Comparison of the average scattering cross-section spectra, $\sigma_b(\lambda)$, at temperatures of 7 and 25°C. (b) Scattering cross-section at 660 nm as a function of temperature. The average value and standard deviation is shown at each temperature. The overall average value of $\sigma_b(660)$ is 3.73×10^{-11} m² cell⁻¹.

values of $b_C^*(660)$ as a function of temperature varied less than 6% about the average value of 3.76 m² (g C)⁻¹.

Light scattering made a significantly greater contribution to beam attenuation than absorption by *T. pseudonana,* which is characteristic for most phytoplankton species. The lowest values of scattering-to-absorption ratio, $b:a,$ which occur in the blue absorption band of Chl *a* at 438 nm, were higher than 5. This ratio showed a consistent decrease with increasing temperature at various wavelengths (not shown here). The largest relative change was observed in the red band of Chl *a,* where $b(674)/a(674)$ decreased more than twofold with temperature.

Effects of nitrogen limitation—The nitrogen-limited chemostat culture was growing at a rate of 0.53 d⁻¹. This value is significantly smaller than the value of 1.36 d⁻¹ for N-replete cells at the same temperature of 20°C and saturating irradiance (Table 2). The major effect of nitrogen limitation on cellular constituents is the increase of C:N and C:Chl *a* (Table 2), resulting primarily from the reduction in N_i and Chl a_i. At the level of the individual cell, the ability to absorb light was reduced in response to N limitation because of a decrease in Chl a_i and n' (Tables 2 and 3). The light scatter was, however, generally enhanced because of an increase in cell size and n (Tables 2 and 3). As a result, the scattering-to-absorption ratio increased significantly under N limitation, for example more than twofold at 674 nm. In contrast, N limitation had a rather small effect on the carbon-specific scattering coefficient (Table 3). The responses to nitrogen limitation demonstrated by the chemostat experiment are consistent with those reported previously for the same species examined in nitrate-limited semicontinuous cultures (Reynolds et al. 1997).

Effects of light limitation—Growth rate, μ, at 25°C was a saturating function of PAR (Fig. 8). The growth rate of cells acclimated to 24 μmol quanta m⁻² s⁻¹ was reduced to 0.64 d⁻¹ compared to 2 d⁻¹ at the saturating irradiance.

The difference in cell size and intracellular carbon between low-light (LL) and high-light (HL) cells is relatively small (Table 2). However, nitrogen and Chl *a* quotas of HL

Table 2. Cell properties of *T. pseudonana* showing the effects of light limitation and N limitation. The effect of light limitation is illustrated by a comparison of the low light and high light data, which were obtained at the same temperature of 25°C under N-replete conditions. The effect of N limitation is illustrated by a comparison of the N-limited and N-replete data, which were obtained at the same temperature of 20°C under saturating irradiances. T is the growth temperature, PAR the growth irradiance, μ the growth rate, G the mean projected area of cells, V the mean cell volume, C_i the intracellular carbon concentration, N_i the intracellular nitrogen concentration, Chl a_i the intracellular chlorophyll *a* concentration, C/N the carbon-to-nitrogen ratio, and C/Chl *a* the carbon-to-chlorophyll *a* ratio. The average values and the coefficient of variation in percent (in parentheses) based on replicate experiments are given.

	T (°C)	PAR (μmol quanta m⁻² s⁻¹)	μ (day⁻¹)	G (μm²)	V (μm³)	C_i (kg m⁻³)	N_i (kg m⁻³)	Chl a_i (kg m⁻³)	C/N (atomic)	C/Chl *a* (g:g)
Low light	25	24	0.64 (36)	16.4 (13)	57.7 (20)	216 (11)	31.8 (11)	10.97 (12)	7.93	20
High light	25	336	2.00 (3)	16.3 (1)	52.5 (4)	203 (9)	22.1 (16)	3.74	10.81	54
N limited	20	410	0.53 (16)	16.8 (11)	59.13 (21)	223 (7)	18.7 (2)	1.01 (9)	13.91	221
N replete	20	340	1.36 (4)	15.3 (14)	48.3 (22)	191 (0.1)	22.1 (2)	2.26*	10.21	85

* Chl *a* determined from the imaginary part of the refractive index (*see text* for details).

Table 3. As Table 2 but comparison is shown for selected optical properties of *T. pseudonana*. $\sigma_a(438)$ is the absorption cross-section at 438 nm, $\sigma_a(674)$ the absorption cross-section at 674 nm, $\sigma_b(660)$ the scattering cross-section at 660 nm, $b_C^*(660)$ the carbon-specific scattering coefficient at 660 nm, $b/a(674)$ the scattering-to-absorption ratio at 674 nm, $n'(674)$ the imaginary part of the refractive index at 674 nm, and $n(660)$ the real part of the refractive index at 660 nm.

	T (°C)	PAR (μmol quanta m^{-2} s^{-1})	$\sigma_a(438)$ (10^{-12} m^2 cell^{-1})	$\sigma_a(674)$ (10^{-12} m^2 cell^{-1})	$\sigma_b(660)$ (10^{-11} m^2 cell^{-1})	$b_C^*(660)$ (m^2 [g C]$^{-1}$)	$b/a(674)$	$n'(674)$ $\times 10^3$	$n(660)$
Low light	25	24	10.93 (10)	8.11 (11)	3.37 (6)	2.75 (3)	3.81 (7)	8.47	1.0434
High light	25	336	5.22 (20)	3.32 (19)	3.83 (8)	3.59 (4)	11.16 (13)	2.90	1.0452
N limited	20	410	3.46 (24)	1.56 (26)	4.72 (12)	3.68 (6)	29.37 (18)	1.13	1.0541
N replete	20	340	4.26 (19)	2.51 (13)	3.60 (18)	3.95 (3)	13.65 (3)	2.35	1.0463

cells were significantly lower than those of LL cells. For example, *Chl* a_i increased nearly threefold from about 3.7 kg m^{-3} in HL cells to 11 kg m^{-3} in LL cells. Both C:N and C:Chl a ratios were higher at saturating irradiance than under light limitation, primarily because of reduced nitrogen and Chl a quotas in HL cells. Consistent with the change in pigment quotas was a decrease in n' and σ_a when cells move from limiting to saturating light (Table 3). The scattering cross-section at 660 nm of LL cells was somewhat lower than that of HL cells, and the $b_C^*(660)$ value of 2.75 m^2 (g C)$^{-1}$ for LL cells was the lowest among all the experiments. Light limitation also resulted in a reduction in the scattering-to-absorption ratio.

Discussion

The response in biochemical composition of *T. pseudonana* to temperature, light, and nitrogen limitation observed
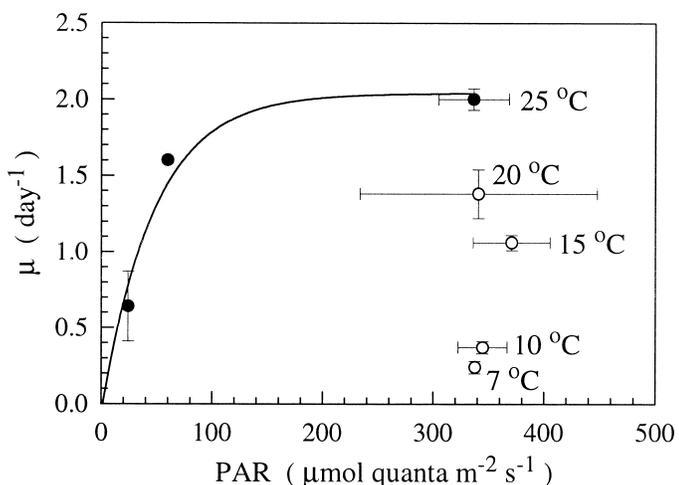

Fig. 8. Specific growth rate, μ, as a function of irradiance, PAR, for *T. pseudonana* grown at 25°C in a nutrient-replete medium (solid circles and the trend line). One of the three data points describing this relationship was obtained from the experiment at PAR = 60 μmol quanta m^{-2} s^{-1}, which is not reported in Tables 1, 2, and 3. For comparison, data obtained at various temperatures (as indicated) under saturating irradiances and nitrogen-replete conditions are also included (open circles). The average values and standard deviations of μ, as well as the range of variation in PAR among replicate experiments, are shown.

in our experiments is consistent with previous studies of this species. For example, the U-shaped pattern of cellular carbon and nitrogen, the linear pattern of increasing C:N, and the general trend of Chl a to increase and C:Chl a to decrease with increasing temperature were observed by Thompson et al. (1992). The reduction in nitrogen and Chl a quotas accompanied by an increase in C:N and C:Chl a ratios for *T. pseudonana* grown either under N limitation or saturating light is also well documented (Eppley and Renger 1974; Berges and Harrison 1995; Reynolds et al. 1997).

The absorption properties of *T. pseudonana* changed significantly in response to a limitation of growth. The effects of temperature and nitrogen limitation on absorption are similar, but they differ distinctly from those of light limitation (Fig. 9). With a reduction in growth rate the absorption cross-section, σ_a, of *T. pseudonana* showed an equivalent decrease regardless of whether the cells were limited by temperature or nitrogen. At the same growth rate the values of $\sigma_a(674)$ within the red band of Chl a were essentially the same for temperature- and nitrogen-limited cells (Fig. 9a). In contrast, $\sigma_a(674)$ increased in response to limitation by light. As a result, the cells growing at a maximum rate under optimal conditions (T = 25°C, saturating light levels and N-replete medium) exhibited intermediate values of $\sigma_a(674)$. The Chl a–specific absorption coefficient, $a_{Chl}^*(674)$, of rapidly growing cells was also intermediate, but, in contrast to $\sigma_a(674)$, the lower values of $a_{Chl}^*(674)$ occurred for light-limited cells and higher values for temperature- and nitrogen-limited cells (Fig. 9b).

The observed patterns in σ_a and a_{Chl}^* result primarily from the acclimative strategies of *T. pseudonana* where there is an increase in Chl a content in response to light limitation and a decrease in Chl a in response to temperature and nitrogen limitation (Sakshaug et al. 1987; Thompson et al. 1992; Reynolds et al. 1997). Changes in the absorption cross-section of cells can be explained in terms of variations in cell size and the imaginary part of the refractive index, n'. The effect of cell size on σ_a is twofold because σ_a equals the product of the projected area of cells, G, and the absorption efficiency factor, Q_a, which also depends on cell size (Bricaud and Morel 1986). However, differences between the mean cell diameter were within 10% among all experiments. While the role of cell size cannot be neglected, most of the observed variation in σ_a can be attributed to n', which affects Q_a. Because n' is proportional to the absorp-
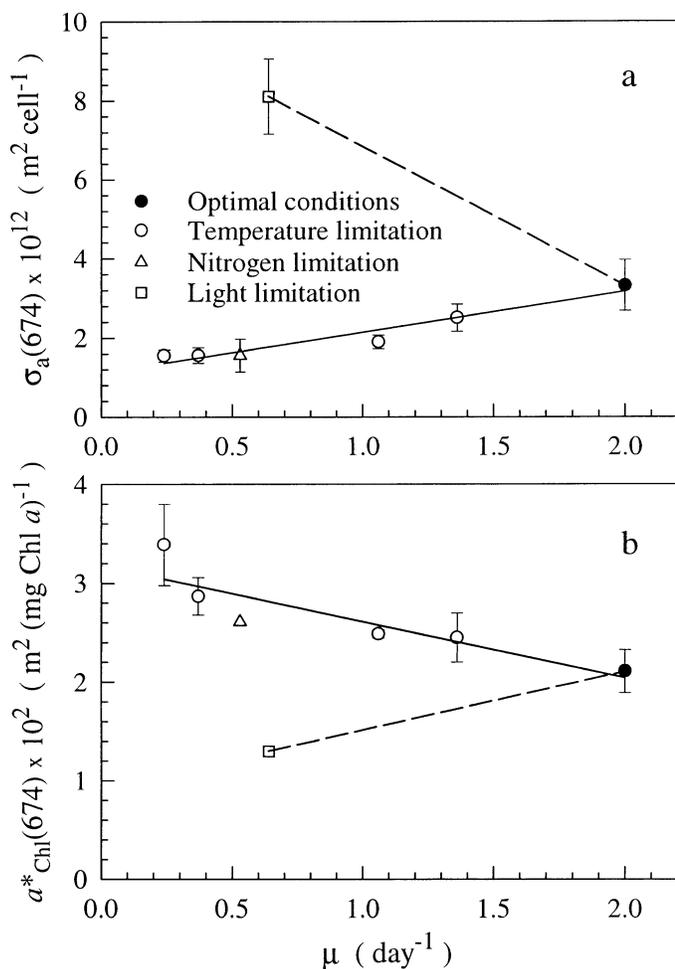
Fig. 10. The imaginary part of the refractive index n' at 674 nm as a function of the intracellular Chl a_i concentration $Chl\ a_i$ for *T. pseudonana* grown under various conditions. Twelve data points for which Chl a was determined by HPLC (*see* text for more details) and the regression line with the corresponding equation are shown. The squared correlation coefficient is 0.998. The data points having the lowest values of the variables represent temperature and nitrogen limitation, the five data points with the highest values are for light limitation, and the intermediate point is for optimal growth conditions. For comparison, the relationships obtained previously for the same species by Stramski and Reynolds (1993) and Reynolds et al. (1997) are also shown (dotted lines).

Fig. 9. (a) Absorption cross-section σ_a at 674 nm as a function of specific growth rate μ for temperature-, nitrogen-, and light-limited *T. pseudonana.* (b) Same as above but for the Chl a–specific absorption coefficient a^*_{Chl} at 674 nm. The chlorophyll data for the three intermediate values of μ under temperature limitation were derived from the imaginary part of the refractive index (*see* text and Fig. 10 for details). The average values and standard deviations are shown at each growth rate, and the data are accompanied by regression lines (the solid line for temperature/nitrogen limitation and the dashed line for light limitation). The regression equations for the combined data representing temperature and nitrogen limitation are $\sigma_a(674) = 1.025 \times 10^{-12}\ \mu + 1.117 \times 10^{-12}$ and $a^*_{Chl}(674) = -0.0057\ \mu + 0.0318$. For light limitation these equations are $\sigma_a(674) = -3.522 \times 10^{-12}\ \mu + 1.036 \times 10^{-11}$ and $a^*_{Chl}(674) = 0.00596\ \mu + 0.00919$.

tion coefficient of cellular matter (Morel and Bricaud 1986), one can expect a correlation between n' and intracellular pigment concentration.

At $\lambda = 674$ nm, where Chl a is a major cause of absorption, $n'(674)$ is well correlated with $Chl\ a_i$ (Fig. 10). The effect of Chl c on $n'(674)$ can be neglected because the intracellular concentration of Chl c (as determined from the HPLC analysis) was only 3 to 7% of that of Chl a and the absorption maximum of Chl c in the red is shifted significantly toward shorter wavelengths compared to the Chl a peak at 674 nm. $Chl\ a_i$ varies 26-fold between the lowest

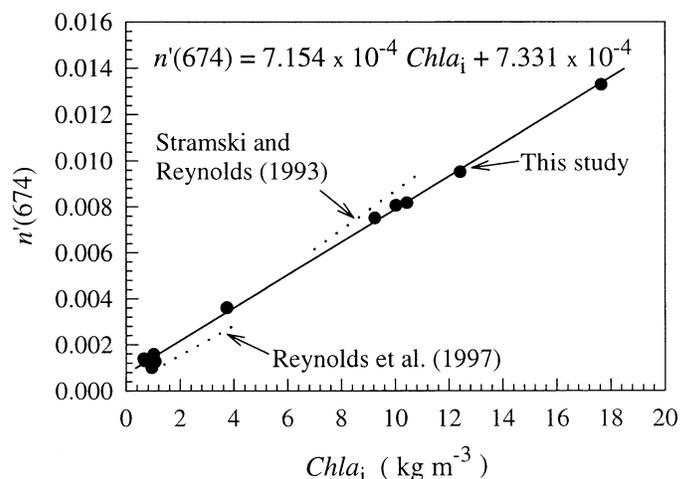values for temperature-limited and nitrogen-limited cells and the highest values for light-limited cells (Fig. 10). This change in $Chl\ a_i$ is accompanied by a 13-fold change in $n'(674)$. Under optimal growth conditions, both $Chl\ a_i$ and $n'(674)$ show intermediate values (*see* the data point corresponding to $Chl\ a_i = 3.74$ kg m^{-3} in Fig. 10). The present relationship between $n'(674)$ and $Chl\ a_i$ agrees quite well with previous data for the same species obtained under a smaller range of growth conditions (Stramski and Reynolds 1993; Reynolds et al. 1997). These results support the idea that $Chl\ a_i$ can be estimated from n', which in turn can be derived from measurements of cell size and absorption within the red peak of Chl a (Stramski 1999).

Changes in Chl a–specific absorption a^*_{Chl} can be caused by variations in the relative abundance of Chl a and accessory pigments and by variations in the package effect. To a first approximation, at the level of whole cells, the package effect increases with the product of the cell diameter D and the spectral absorption coefficient of cellular matter $a_{cm}(\lambda)$ (Morel and Bricaud 1981). The coefficient $a_{cm}(\lambda)$ is proportional to $n'(\lambda)$, and therefore to the intracellular pigment concentration according to the results discussed above. Because absorption by accessory pigments at 674 nm is minimal, the package effect is expected to account for nearly all the change in $a^*_{Chl}(674)$. Our data combining all the sources of growth limitation show an inverse relationship between $a^*_{Chl}(674)$ and the product $Chl\ a_i\ D$ (Fig. 11). This result is consistent with models of pigment packaging (Morel and Bricaud 1981) and previous data (e.g., Sosik and Mitchell 1994; Reynolds et al. 1997).

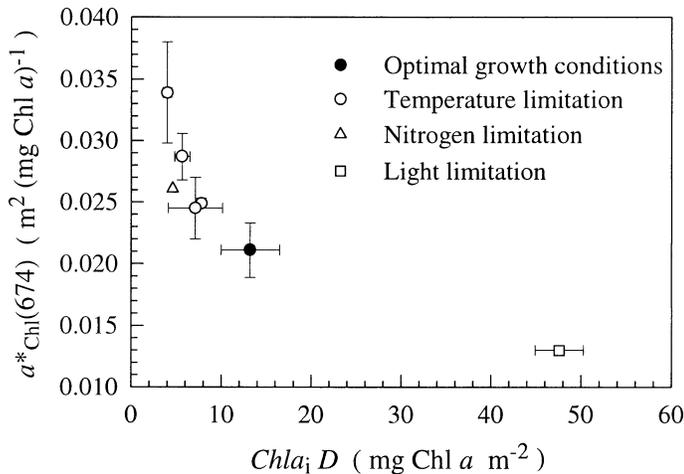The light-limited cells show the highest values of the

Fig. 11. The relationship between the Chl a–specific absorption coefficient a^*_{Chl} at 674 nm and the product $Chl\ a_i\ D$, where $Chl\ a_i$ is the intracellular concentration of Chl a and D is the mean cell diameter. The average values and standard deviations for both variables are shown. The chlorophyll data for the three intermediate data points shown as open circles were obtained from the imaginary part of the refractive index (*see* text and Fig. 10 for details).

product $Chl\ a_i\ D$, and consequently the greatest reduction of $a^*_{Chl}(674)$ due to the package effect. The package effect in light-limited phytoplankton has been well documented by numerous studies (Berner et al. 1989; Johnsen et al. 1994; Moisan and Mitchell 1999). Under optimal growth conditions, our estimate of $a^*_{Chl}(674)$ was, on average, 0.0211 m² (mg Chl a)⁻¹, which is close to the commonly accepted value of 0.0202 m² (mg Chl a)⁻¹ for Chl a dissolved in 90% acetone at $\lambda = 664$ nm (Jeffrey and Humphrey 1975). Previous studies suggested that this value may provide a close approximation to the maximum unpackaged absorption by *Thalassiosira* species in the red band of Chl a (Geider and Osborne 1987; Stramski and Reynolds 1993; Reynolds et al. 1997). However, the temperature- and nitrogen-limited cells in this study exhibited $a^*_{Chl}(674)$ values higher than 0.02 m² (mg Chl a)⁻¹ (Fig. 11).

Under nitrogen-limited conditions, $a^*_{Chl}(674)$ was about 0.026 m² (mg Chl a)⁻¹, which suggests a very weak, perhaps negligible, package effect due to low intracellular pigment concentration. This trend is consistent with previous observations of *T. pseudonana* (Reynolds et al. 1997) and the marine chlorophyte *Dunaliella tertiolecta* (Sosik and Mitchell 1991) under nitrogen limitation. At the slowest growth rate that occurred at a temperature of 7°C, *T. pseudonana* exhibited the highest values of $a^*_{Chl}(674)$ of about 0.034 m² (mg Chl a)⁻¹, which also suggests a very weak, if any, package effect (note a relatively large standard deviation of 0.004 m² [mg Chl a]⁻¹ in this case). This observation of a reduction in the package effect with decreasing growth temperature is also consistent with a previous study of *Dunaliella tertiolecta* (Sosik and Mitchell 1994). Although many values of $a^*_{Chl}(674)$ reported in literature for various phytoplankters grown in cultures are lower than our estimates for nutrient- and temperature-limited *T. pseudonana*, there exists evidence that unpackaged $a^*_{Chl}(674)$ can be higher than a value
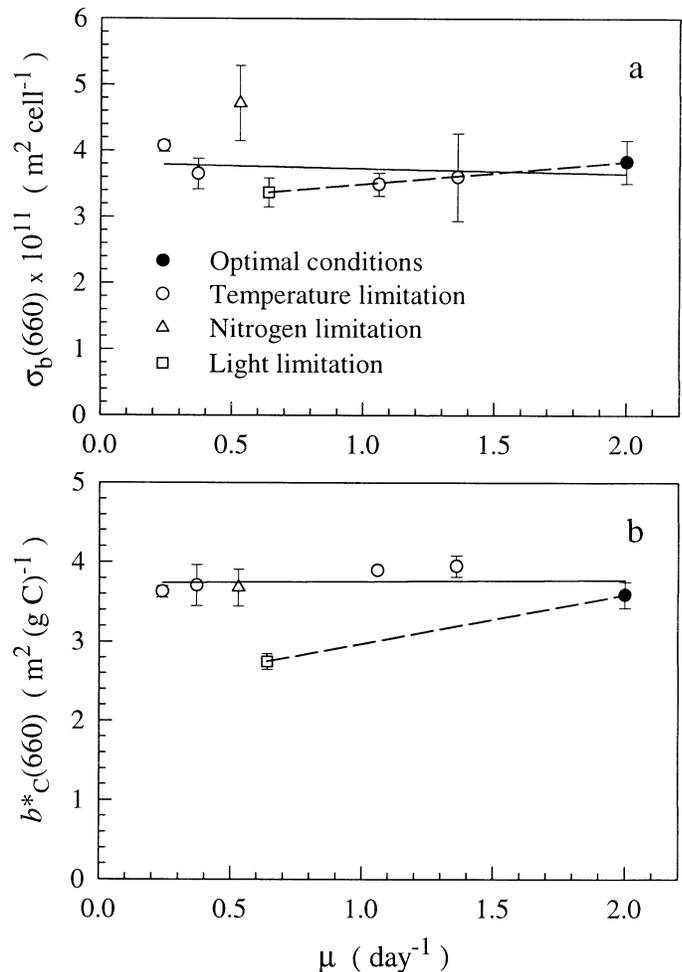

Fig. 12. (a) Scattering cross-section σ_b at 660 nm as a function of specific growth rate μ for temperature-, nitrogen-, and light-limited *T. pseudonana*. (b) Same as above but for the carbon-specific scattering coefficient b^*_C at 660 nm. The average values and standard deviations are shown at each growth rate, and the data are accompanied by trend lines (the solid line for temperature limitation/nitrogen and the dashed line for light limitation).

of 0.02 m² (mg Chl a)⁻¹ for Chl a in 90% acetone. By measuring the disrupted-cell absorption spectra of dinoflagellates, Johnsen et al. (1994) found that maximum unpackaged $a^*_{Chl}(674)$ at 675 nm is close to 0.027 m² (mg Chl a)⁻¹. Other studies also provided estimates of unpackaged $a^*_{Chl}(674)$ in the range 0.02–0.03 or even above 0.03 m² (mg Chl a)⁻¹ (Morel and Bricaud 1981; Sathyendranath et al. 1987; Nelson and Prézelin 1990). Our estimates for nutrient- and temperature-limited *T. pseudonana* are within that range. It appears that under severe temperature stress the coefficient $a^*_{Chl}(674)$ of *T. pseudonana* is higher and the package effect weaker than for other growth conditions.

The scattering cross-section σ_b varied as a function of growth rate to a much lesser extent than absorption (Fig. 12a). To a first approximation, one could use an average value of $\sigma_b(660) = 3.8 \times 10^{-11}$ m² cell⁻¹ derived from all the experiments for any growth rate regardless of the source of growth limitation. The nitrogen-limited cells showed the

highest value of $\sigma_b(660)$. The difference between the average $\sigma_b(660)$ for these cells and the overall average value of $\sigma_b(660)$ based on all the experiments is 25%, but the standard deviation for the chemostat culture was quite large, suggesting that this difference may in fact be smaller. In addition, previous observations also suggested that scattering cross-sections are not a strong function of nitrogen-limited growth rate for this species (Reynolds et al. 1997). However, σ_b of *T. pseudonana* was shown to vary significantly over a diel cycle in irradiance (Stramski and Reynolds 1993).

The scattering cross-section σ_b is the product of G and Q_b, where the scattering efficiency factor Q_b depends in a rather complicated fashion on cell size, the real part of the refractive index, and the imaginary part of the index (Morel and Bricaud 1986). At 660 nm, the effect of n' is small and, to a first approximation, we can interpret $\sigma_b(660)$ in terms of cell size and $n(660)$. For example, variations in $\sigma_b(660)$ as a function of temperature-dependent growth rate are small (Fig. 12a) because an increase in cell size with temperature (Fig. 3) and a decrease in refractive index with temperature (Fig. 5) compensate each other.

The carbon-specific scattering at 660 nm, $b_C^*(660)$, was nearly independent of growth rate for various temperatures and nitrogen-limitation conditions (Fig. 12b). The average value based on these experiments is 3.745 m² (g C)⁻¹. The light-limited cells showed, however, a lower value ($\sim$2.75 m² [g C]⁻¹) because these cells had a relatively low $\sigma_b(660)$ ($\sim$3.4 × 10⁻¹² m² cell⁻¹) and relatively high cellular carbon content ($\sim$12.5 pg C per cell). The C-specific beam attenuation coefficient, $c_C^*(660)$, was 3.13 m² (g C)⁻¹ for light-limited cells and 3.85 ($\pm$0.063) m² (g C)⁻¹ for all the other growth conditions. Ackleson et al. (1993) also suggested that c_C^* appears to be sensitive to growth irradiance. In spite of that, our results show that variations in $c_C^*(660)$ induced by large changes in growth conditions are limited to within about 20% for *T. pseudonana*. This range is somewhat greater compared to previous average estimates of $c_C^*(660)$ for this species, which were 3.81 m² (g C)⁻¹ in the diel experiment (Stramski and Reynolds 1993) and 3.47 m² (g C)⁻¹ in a nitrate-limitation experiment (Reynolds et al. 1997). Documenting and understanding variability in carbon-specific attenuation is especially important because beam attenuation may serve as a proxy for the particulate organic carbon concentrations in the ocean (Gardner et al. 1993; Marra et al. 1995; Bishop 1999). Measurements of beam attenuation on the diel timescale also have the potential to provide estimates of oceanic primary productivity and particle dynamics (Siegel et al. 1989). Variable c_C^* could confound these applications (e.g., Ackleson et al. 1993; Cullen and Lewis 1995) and more efforts are needed to examine the possible variations in c_C^* in various planktonic species.

While the imaginary part of the refractive index shows a strong correlation with intracellular Chl *a*, equally interesting are the results of the real part of the refractive index, *n*, and the intracellular carbon concentration, C_i. We observed a significant correlation between $n(660)$ and C_i for *T. pseudonana* (Fig. 13), which results from the fact that *n* depends primarily on fractional volumes of water and solid matter within a cell. As compared to earlier studies of *T. pseudonana*, $n(660)$ and C_i exhibited a relatively large variation due to a
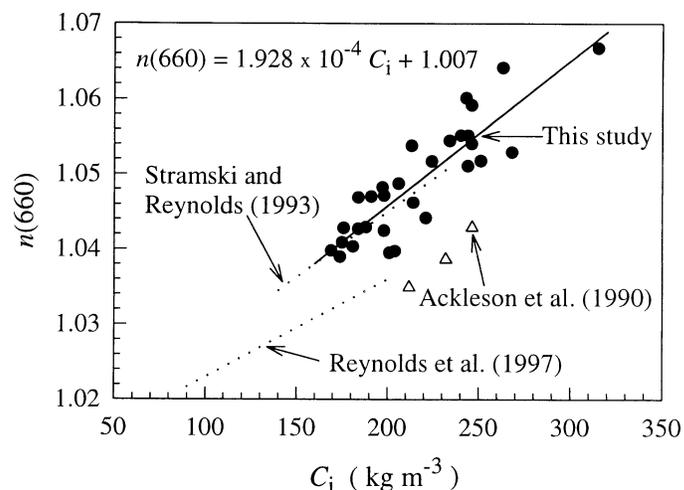

Fig. 13. The real part of the refractive index *n* at 660 nm as a function of the intracellular concentration of organic carbon, C_i, for *T. pseudonana*. Included are 30 data points (solid circles) from all the experiments under various growth conditions (including experiments at intermediate PAR not shown in Table 1 and other replicate experiments excluded from Table 1 because of incomplete suite of measurements). The solid line depicts the best-fit regression to these data and the corresponding equation is also displayed. The squared correlation coefficient is 0.77. For comparison, previous data (Ackleson et al. 1990) and relationships (Stramski and Reynolds 1993; Reynolds et al. 1997) obtained for the same species are also shown, as indicated.

broad range of growth conditions. The present relationship compares very well with previous results obtained under a day–night cycle in irradiance (Stramski and Reynolds 1993). However, other data for this species (Ackleson et al. 1990; Reynolds et al. 1997) show lower values of the refractive index for any given intracellular carbon. No specific cause for this disagreement has been identified, but possible explanations include differences in both cell properties and experimental methods among the various studies. For example, while Ackleson et al. (1990) determined the refractive index from flow cytometry measurements of light scatter by single cells, the remaining data in Fig. 13 were obtained from bulk optical measurements on cell suspensions. Importantly, in both cases the refractive index was not measured directly but was estimated from inverse methods, which should be regarded merely as a practical way of providing approximate characterization of the bulk refractive index of cells rather than the actual true value of the index. In addition, such inverse methods involve several sources of uncertainties associated with optical measurements, particle size measurements, and the optical theory used to match the measurements, which in these cases was based on the assumption of sphericity and internal homogeneity of cells. Nevertheless, the observed degree of correlation between *n* and C_i provides a motivation for further studies, especially because this relation promises a unique capability to determine cellular carbon from optical measurements (Stramski 1999).

In conclusion, this study confirms that significant changes in the optical properties of phytoplankton can be induced by temperature-, nutrient-, and light-limited growth conditions.

Our results suggest that unifying descriptions for the effects of temperature and nitrogen limitation on the absorption properties, σ_a and a^*_{Chl}, as a function of growth rate μ may be suitable for *T. pseudonana*. Variability in σ_a and a^*_{Chl} with light-limited growth rate is, however, distinctively different. The results for scattering cross-sections σ_b (Fig. 12) offer a temptingly simple hypothesis that phytoplankton cells will exhibit similar values of σ_b (within the spectral bands of weak or negligible absorption) at the same growth rate, regardless of the source of growth limitation. This would require that cells growing at a certain rate have similar size and a real part of refractive index regardless of the source of growth limitation. Although in our study $\sigma_b(660)$ of *T. pseudonana* remained nearly invariant with growth rate, we recognize that σ_b may change significantly with μ for other species or may show significant diel variability. It is evident that further studies of the responses of a wide range of species to various sources of growth limitation are needed to adequately understand optical variability in the ocean associated with acclimative strategies of phytoplankton.

It is of interest to note that models of phytoplankton growth were recently developed to describe dynamic interactions of light, nutrients, and temperature (e.g., Geider et al. 1998). One problem that precludes a mechanistic linkage of the existing growth models to the detailed optical characterization of phytoplankton is that these models do not predict variations in cell size distribution and complex refractive index, the major determinants of particle optics. For example, the Geider et al. (1998) model predicts the growth rate and the ratios Chl a : C, Chl a : N, and N : C. In an ideal case, if a phytoplankton model was capable of predicting cell size and cellular contents of Chl a and C, one could derive the complex refractive index from relationships such as those shown in Figs. 10 and 13 and then estimate the optical properties of cells. Certainly, this approach would still have limitations, for example the spectral behavior of optical properties could be difficult to predict with good accuracy. Our results summarized in Figs. 9 and 12 can be viewed as one alternative approach to linking optics and growth models, which is based on empirical relationships between the optical properties and the growth rate instead of a direct mechanistic linkage via cell size and refractive index. We also note that detailed studies of phytoplankton optics can complement growth models by aiding in parameterization of optical variables (e.g., a^*_{Chl}) or validation of such parameterizations.

References

ACKLESON, S. G., J. J. CULLEN, J. BROWN, AND M. P. LESSER. 1990. Some changes in the optical properties of marine phytoplankton in response to high light intensity, p. 238–249. *In* R. W. Spinrad [ed.], Ocean Optics X. SPIE Proceedings 1302.

———, ———, ———, AND ———. 1993. Irradiance-induced variability in light scatter from marine phytoplankton in culture. J. Plankton Res. **15:** 737–759.

AHN, Y.-H., A. BRICAUD, AND A. MOREL. 1992. Light backscattering efficiency and related properties of some phytoplankters. Deep-Sea Res. **39:** 1835–1855.

BALCH, W. M., D. T. DRAPEAU, T. L. CUCCI, R. D. VILLANCOURT, K. A. KILPATRICK, AND J. J. FRITZ. 1999. Optical backscatter-ing by calcifying algae: Separating the contribution of particulate inorganic and organic carbon fractions. J. Geophys. Res. **104:** 1541–1558.

BERGES, J. A., AND P. J. HARRISON. 1995. Relationships between nitrate reductase activity and rates of growth and nitrate incorporation under steady-state light or nitrate limitation in the marine diatom *Thalassiosira pseudonana* (Bacillariophyceae). J. Phycol. **31:** 85–95.

BERNARD, O., G. MALARA, AND A. SCIANDRA. 1996. The effects of a controlled fluctuating nutrient environment on continuous cultures of phytoplankton monitored by computers. J. Exp. Mar. Biol. Ecol. **197:** 263–278.

BERNER, T., Z. DUBINSKY, K. WYMAN, AND P. G. FALKOWSKI. 1989. Photoadaptation and the "package" effect in *Dunaliella tertiolecta* (Chlorophyceae). J. Phycol. **25:** 70–78.

BISHOP, J. K. B. 1999. Transmissometer measurement of POC. Deep-Sea Res. I **46:** 353–369.

BOHREN, C. F., AND D. R. HUFFMAN. 1983. Absorption and scattering of light by small particles. Wiley.

BRAND, L. E., L. S. MURPHY, R. R. L. GUILLARD, AND T. H. LEE. 1981. Genetic variability and differentiation in the temperature niche component of the diatom *Thalassiosira pseudonana*. Mar. Biol. **62:** 103–110.

BRICAUD, A., A.-L. BÉDHOMME, AND A. MOREL. 1988. Optical properties of diverse phytoplanktonic species: Experimental results and theoretical interpretation. J. Plankton Res. **10:** 851–873.

———, AND A. MOREL. 1986. Light attenuation and scattering by phytoplanktonic cells: A theoretical modeling. Appl. Opt. **25:** 571–580.

———, ———, AND L. PRIEUR. 1983. Optical efficiency factors of some phytoplankters. Limnol. Oceanogr. **28:** 816–832.

CULLEN, J. J., AND M. R. LEWIS. 1995. Biological processes and optical measurements near the surface: Some issues relevant to remote sensing. J. Geophys. Res. **100:** 13255–13266.

EPPLEY, R. W., AND E. H. RENGER. 1974. Nitrogen assimilation of an oceanic diatom in nitrogen-limited continuous culture. J. Phycol. **10:** 15–23.

GARDNER, W. D., I. D. WALSH, AND M. J. RICHARDSON. 1993. Biophysical forcing of particle production and distribution during a spring bloom in the North Atlantic. Deep-Sea Res. II **40:** 171–195.

GEIDER, R. J., H. L. MACINTYRE, AND T. M. KANA. 1998. A dynamic regulatory model of phytoplanktonic acclimation to light, nutrients, and temperature. Limnol. Oceanogr. **43:** 679–694.

———, AND B. A. OSBORNE. 1987. Light absorption by a marine diatom: Experimental observations and theoretical calculations of the package effect in a small *Thalassiosira* species. Mar. Biol. **96:** 299–308.

GUILLARD, R. R., AND J. H. RYTHER. 1962. Studies of marine planktonic diatoms. 1. *Cyclotella nana* Hustedt and *Detonula confervacea* (Cleve) Gran. Can. J. Microbiol. **8:** 229–239.

JEFFREY, S. W., AND G. F. HUMPHREY. 1975. New spectrophotometric equations for chlorophylls a, b, c_1, and c_2 in higher plants, algae and natural phytoplankton. Biochem. Physiol. Pflanz. **167:** 191–194.

JOHNSEN, G., N. B. NELSON, R. V. M. JOVINE, AND B. B. PRÉZELIN. 1994. Chromoprotein- and pigment-dependent modeling of spectral light absorption in two dinoflagellates, *Prorocentrum minimum* and *Heterocapsa pygmaea*. Mar. Ecol. Prog. Ser. **114:** 245–258.

KIEFER, D. A. 1973. Chlorophyll a fluorescence in marine centric diatoms: Responses of chloroplasts to light and nutrient stress. Mar. Biol. **23:** 39–46.

MALARA, G., AND A. SCIANDRA. 1991. A multiparameter phyto-

planktonic culture system driven by microcomputer. J. Appl. Phycol. **3:** 235–241.

Mantoura, R. F. C., and D. J. Repeta. 1997. Calibration methods for HPLC, 407–428. *In* R. F. C. Mantoura, S. W. Jeffrey, and S. W. Wright [eds.], Phytoplankton pigments in oceanography: Guidelines to modern methods. UNESCO.

Marra, J., C. Langdon, and C. A. Knudson. 1995. Primary production, water column changes, and the demise of a *Phaeocystis* bloom at the marine light-mixed layers site (59°N, 21°W) in the northeast Atlantic Ocean. J. Geophys. Res. **100:** 6633–6643.

Moisan, T. A., and B. G. Mitchell. 1999. Photophysiological acclimation of *Phaeocystis antarctica* Karsten under light limitation. Limnol. Oceanogr. **44:** 247–258.

Moore, L. R., R. Goericke, and S. W. Chisholm. 1995. Comparative physiology of *Synechococcus* and *Prochlorococcus:* Influence of light and temperature on growth, pigments, fluorescence and absorptive properties. Mar. Ecol. Prog. Ser. **116:** 259–275.

Morel, A., and A. Bricaud. 1981. Theoretical results concerning light absorption in a discrete medium, and application to specific absorption of phytoplankton. Deep-Sea Res. **28:** 1375–1393.

———, and ———. 1986. Inherent optical properties of algal cells including picoplankton: Theoretical and experimental results, p. 521–555. *In* T. Platt and W. K. W. Li [eds.], Photosynthetic picoplankton. Can. Bull. Fish. Aquat. Sci. 214.

Nelson, N. B., and B. B. Prézelin. 1990. Chromatic light effects and physiological modeling of absorption properties of *Heterocapsa pygmaea* (= *Glenodinium sp.*). Mar Ecol. Prog. Ser. **63:** 37–46.

Reynolds, R. A., D. Stramski, and D. A. Kiefer. 1997. The effect of nitrogen limitation on the absorption and scattering properties of the marine diatom *Thalassiosira pseudonana.* Limnol. Oceanogr. **42:** 881–892.

Sakshaug, E., S. Demers, and C. M. Yentsch. 1987. *Thalassiosira oceanica* and *T. pseudonana*: Two different photoadaptational responses. Mar. Ecol. Prog. Ser. **41:** 275–282.

Sathyendranath, S., L. Lazzara, and L. Prieur. 1987. Variations in the spectral values of specific absorption of phytoplankton. Limnol. Oceanogr. **32:** 403–415.

Siegel, D. A., T. D. Dickey, L. Washburn, M. K. Hamilton, and B. G. Mitchell. 1989. Optical determination of particulate abundance and production variations in the oligotrophic ocean. Deep-Sea Res. **36:** 211–222.

Sosik, H. M., and B. G. Mitchell. 1991. Absorption, fluorescence, and quantum yield for growth in nitrogen-limited *Dunaliella tertiolecta.* Limnol. Oceanogr. **36:** 910–921.

———, and ———. 1994. Effects of temperature on growth, light absorption, and quantum yield in *Dunaliella tertiolecta* (Chlorophyceae). J. Phycol. **30:** 833–840.

Stramski, D. 1999. Refractive index of planktonic cells as a measure of cellular carbon and chlorophyll *a* content. Deep-Sea Res. I **46:** 335–351.

———, and A. Morel. 1990. Optical properties of photosynthetic picoplankton in different physiological states as affected by growth irradiance. Deep-Sea Res. **37:** 245–266.

———, ———, and A. Bricaud. 1988. Modeling the light attenuation and scattering by spherical phytoplanktonic cells: A retrieval of the bulk refractive index. Appl. Opt. **27:** 3954–3957.

———, and R. A. Reynolds. 1993. Diel variations in optical properties of a marine diatom. Limnol. Oceanogr. **38:** 1347–1364.

Thompson, P. A., M. X. Guo, and P. J. Harrison. 1992. Effects of variation in temperature. I. On the biochemical composition of 8 species of marine phytoplankton. J. Phycol. **28:** 481–488.

van de Hulst, H. C. 1957. Light scattering by small particles. Wiley.

Vidussi, F., H. Claustre, J. Bustillos-Guzmàn, C. Cailliau, and J.-C. Marty. 1996. Rapid HPLC method for determination of phytoplankton chemotaxinomic pigments: Separation of chlorophyll a from divinyl-chlorophyll a and zeaxanthin from lutein. J. Plankton Res. **18:** 2377–2382.

Volten, H., J. F. de Haan, J. W. Hovenier, R. Schreurs, W. Vassen, A. G. Dekker, H. J. Hoogenboom, F. Charlton, and R. Wouts. 1998. Laboratory measurements of angular distributions of light scattered by phytoplankton and silt. Limnol. Oceanogr. **43:** 1180–1197.